ACS APPLIED MATERIALS & INTERFACES

Research Article

www.acsami.org

Origin of the Increased Photocatalytic Performance of TiO_2 Nanocrystal Composed of Pure Core and Heavily Nitrogen-Doped Shell: A Theoretical Study

Xiangchao Ma,[†] Ying Dai,*[,†] and Baibiao Huang[‡]

[†]School of Physics, State Key Lab of Crystal Materials, Shandong University, Jinan 250100, China

[‡]State Key Lab of Crystal Materials, Shandong University, Jinan 250100, China

ABSTRACT: We have carried out a theoretical study to explain the photocatalytic performance of the newly synthesized special core (pure TiO_2)−shell (heavily nitrogen (N)-doped TiO_2) structure of TiO_2 nanocrystal using advanced first-principles calculations. The conventional N doping models by maximizing the mutual distances between dopants are found to only introduce localized gap states irrespective of doping concentrations, which is in agreement with previous theoretical results but cannot explain the experimental results. In comparison, the electronically coupled N doping of TiO_2, which is almost as stable as the conventional doping models and generally overlooked in previous works, can not only narrow the overall band gap but also decrease the carrier recombination rate. In particular, in the special core−shell structure of TiO_2 nanocrystal, perfect type-II-like homojunction is formed, which can further decrease the carrier recombination rate. The present study conclusively accounts for the recent experimental results and indicates that the final electronic structures of doping system are very sensitive to the models used to conduct calculations, which can rationalize the distinct conclusions about N-doped TiO_2 in previous theoretical works.

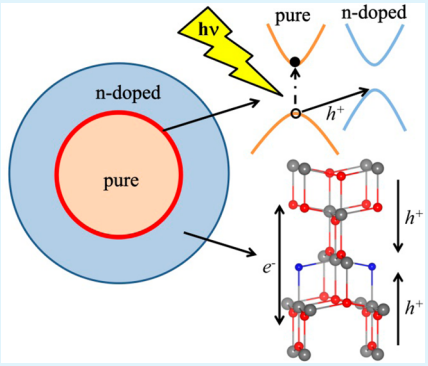

KEYWORDS: *photocatalysis, N-modified TiO_2, electronic structures, homojunction, core−shell structure*

INTRODUCTION

Developing a photocatalyst, which can effectively absorb solar light and transfer the photogenerated carriers from bulk region to surface reaction sites, has always been crucial for efficient solar energy conversion into chemical energy and electricity, and for photodecomposition of organic molecules, such as water and air purifications.[1−3] Being abundant, nontoxic, and stable in the photocatalytic process, titanium dioxide (TiO_2) is considered as the most promising solar-driven photocatalyst. However, the intrinsic drawbacks of TiO_2, including its large energy band gap which impedes exploitation of wide-range solar light, and the low quantum efficiency because of high recombination rate of photogenerated carries, significantly hamper its practical applications. In the past decades, many efforts have been devoted to improving such situations.[4−6] For example, doping in TiO_2 with almost every metal and nonmetal element in the periodic table has been investigated both experimentally and theoretically.[5,7−11] In particular, nitrogen (N) has been demonstrated as an effective dopant to enhance the photocatalytic performance of TiO_2.[8,12−15] However, the effects of N doping on the electronic structures of TiO_2 are still a matter of debate, and there exist long-standing controversies among theoretical scientists. Overall, there are mainly three different points of view about the effects of N doping on the electronic structures of TiO_2: (1) In the original work of Asahi et al.,[8] their elementary calculations based on LDA-FLAPW show that N doping decreases the overall band gap of TiO_2 by widening the valence band. (2) Most of the following theoretical studies show that N doping only introduces localized gap states, without altering either the host valence band edge (Ev) or conduction band edge (Ec) irrespective of doping concentrations.[16,17] (3) In 2011, from the perspective of thermodynamics, J. B. Varley et al. concluded that substitutional N is a deep acceptor, which gives rise to sub-bandgap impurity-to-band transitions in the visible range.[18]

Very recently, Lin et al. developed a facile method to realize high-concentration N doping in TiO_2.[14] Because of their special preparation method, the core region of TiO_2 particle cannot be doped and thus remains pure, while the shell region is heavily doped with N. By the way, we note that such special core−shell structures of TiO_2, in which the shell is heavily doped with other elements, have also been prepared recently.[19] As a result, such TiO_2 nanocrystal shows significantly increased photocatalytic performance under both ultraviolet and visible light irradiations. Also, the photoluminescence (PL) spectra of N-doped TiO_2 show that the recombination rate of photogenerated electrons and holes under ultraviolet irradiation is significantly decreased. In addition, the corresponding Ev is also

Received: October 12, 2014
Accepted: December 3, 2014
Published: December 3, 2014

elevated, as revealed by the X-ray photoelectron spectroscopy (XPS) valence band spectra. However, it is hard to explain these phenomena using existing theories. As listed above, even though viewpoints 2 and 3 may explain the increased photocatalytic performance under visible light, they cannot account for the reduced recombination rate of carriers under ultraviolet light, since the gap states introduced in the heavily N-doped shell region generally lead to increased recombination rate of photogenerated carriers. It seems that viewpoint 1 may explain such phenomena: the reduced overall band gap can increase the visible light absorption, resulting in enhanced photocatalytic performance; the narrowed band gap of N-doped shell might also make it form type-II band alignment with the pure core, which can decrease the recombination of photogenerated carriers under ultraviolet irradiation, thus increasing the photocatalytic performance.

Nevertheless, given the significant approximation of the methods used by Asahi et al.[8] and the disparities among existing results, in the present work, we re-examine the effects of N doping on the electronic structures of TiO_2 using advanced hybrid density functional calculations and considering all of the possible N arrangements in TiO_2 lattice. On the basis of such calculations, we aim at rationalizing the high photocatalytic performance of the special core−shell structure of TiO_2 nanocrystals prepared by Lin et al. and uncovering the reasons that lead to different theoretical results about N-doped TiO_2. In addition, some general effects of the special core−shell structure of TiO_2 on photocatalytic performance are discussed.

COMPUTATIONAL METHODS

We carry out the density functional theory (DFT) calculations using the projector augmented wave (PAW) pseudopotentials within the generalized-gradient approximation (GGA) functional of Perdew, Becke, and Ernzerhof (PBE), as implemented in the Vienna *ab initio* Simulation Package (VASP) code.[20,21] Such calculations based on GGA are known to give accurate groundstate atomic structures; however, they significantly underestimate the band gap, which may affect the accurate description of defect states. Therefore, to provide good physical descriptions of defects, Heyd−Scuseria−Ernzerhof (HSE) hybrid functional is used in our calculations of electronic structures.[22,23] The experimental lattice parameters [a = 3.776 Å, c/a = 2.512] are used to simulate bulk TiO_2. N doping in different concentrations is modeled by replacing one oxygen atom in 3 × 3 × 1, 2 × 2 × 1, and 1 × 1 × 1 supercells, respectively. We stress that both the conventional doping methods by maximizing the mutual distances between dopants and the electronically coupled doping method are considered for heavy doping concentration. The electron wave function is expanded in plane waves up to a cutoff energy of 400 eV. Also, the Brillouin zones of the 3 × 3 × 1, 2 × 2 × 1, and 1 × 1 × 1 supercells are modeled with 3 × 3 × 4, 4 × 4 × 3, and 7 × 7 × 3 Γ-centered k-points,[24] respectively. All of these setups are shown to provide sufficient precision. The atomic positions of all atoms are fully relaxed until the residual forces are smaller than 0.02 eV/Å. The total and projected densities of states are calculated at the equilibrium volume using the tetrahedron method with Blöchl corrections for accuracy.[25] When examining the relative positions of valence and conduction band edges, the 3s levels of Ti atoms far away from the doped N atoms, which are practically at the same energy in pure and N-doped models,[16] are aligned to each other.

Since in HSE functional the exchange potential is divided into a short-range Hartree−Fock (HF) and PBE mixed part and a long-range PBE part, and the percentage of HF in the short-range part often depends on specific system, a systematic survey is needed for anatase TiO_2. It is shown that a proportion of 20% HF exchange mixed with 80% PBE exchange produces the experimental band structures, which is thus used for our present calculations.[37] In addition, because N-doped models have unpaired electrons, spin-polarized calculations are conducted, and the most stable magnetic configurations are used for further calculations.

The molecular dynamics (MD) calculations are performed with a 2 fs time step. The 3 × 3 × 1 supercell models consisting of 108 atoms are used for the three doping cases as shown in Figure 2, which are brought to 300 K during a 2 ps equilibration run. A canonical ensemble is simulated using the algorithm of Nosé.[26,27] Note that, during the MD run, the conventional GGA-PBE functional rather than HSE functional is used, since the HSE functional is computationally very expensive.

RESULTS AND DISCUSSION

Experimentally, the XPS measurements showed that N substitutionally occupies the O site and bonds with Ti.[14] Thus, we substitute N for O to construct the N-doped TiO_2 models. Generally speaking, given the possible electrostatic repulsion between doping atoms, the models for N doping in TiO_2 are constructed to maximize the mutual distances between dopants.[16,17] In addition to taking such conventional wisdom into account, since anatase TiO_2 lattice can be structurally regarded as stack of Ti−O−Ti chains along the crystal c axis (Figure 1), we also construct N doping along one

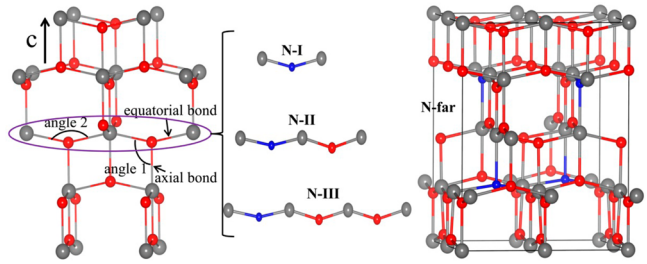

Figure 1. Crystal structures of anatase TiO_2 (on the left) and the periodic units for the three doping arrangements along the Ti−O−Ti chain (in the middle); on the right we show the doping model of N-far, which is in the same doping concentration as N-I but has the mutual distances between dopants maximized. The gray, red, and blue balls represent Ti, O, and N atoms, respectively.

of such chains. Also, three representative doping models, denoted as N-I, N-II, and N-III, respectively, are considered, as shown in Figure 1. These three models correspond to the atomic doping concentrations of 8.33 at. %, 2.08 at. %, and 0.93 at. %, respectively. Here, we point out that because the dopant arrangements in N-II and N-III models are very similar to those in the conventional doping models with the same doping concentrations, only the conventional doping model with the same doping concentration as N-I is further constructed for comparison, which is denoted as N-far in Figure 1. As we can see, for the heavy doping concentration of 8.33 at. %, the conventional doping model N-far is very different from N-I proposed in this work. Our survey shows that N-I is almost as stable as N-far, with the latter one being only 0.045 eV per unit cell (Note that this value comes from calculations using the GGA-PBE functional) more stable. Thus, from the viewpoint of thermodynamic equilibrium, the heavy doping model N-I considered here, which is generally overlooked theoretically, should also exist in quite a large amount in the real doping samples, especially considering the high annealing temperature during the preparation process. Additionally, concerns about possible phase separation in heavy doping models can be excluded, since high concentration N doping of TiO_2 up to 8 at. % and even 10 at. % has been experimentally realized.[13,28]

Because the regular arrangement of N dopants in N-I renders it a low entropy structure, which might be unstable, we further conduct MD studies of N-I doping model. As shown in Figure 2a, the doped structure of N-I in 300 K is quite stable,

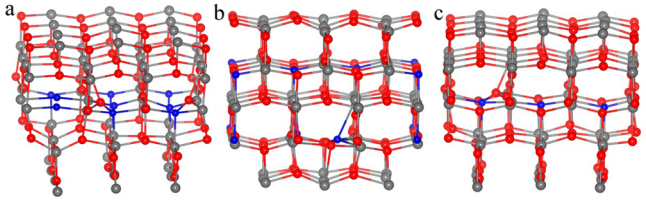

Figure 2. Typical geometric structures during MD calculations in 300 K. (a) N-I doping model. (b and c) Doping models where the mutual distances between dopants are maximized and where lower concentration of Ti−N−Ti chains is introduced, respectively.

indicating the doping model is actually reasonable. Additionally, one can note that there is N−O bonding in Figure 2a. This is because the conventional GGA-PBE functional is used in MD calculations, which overly delocalizes the O and N p orbitals[29] and thus spuriously enhances their interactions through p orbitals. As we can see, such spurious interactions are also observed in doping models where the mutual distances between dopants are maximized (Figure 2b) and where lower concentration of Ti−N−Ti chains is introduced (Figure 2c). Experimentally, preparing the doping structure of N-far is very easy. In comparison, at first sight, one may think that it is hard or even impossible to prepare the doping structure of N-I experimentally. However, our calculations show that when a substitutional N atom is introduced into TiO_2, it can make the formation of oxygen vacancy, which is adjacent to the N atom and in the same Ti−O−Ti chain as the N atom, much easier than that far away from the N atom and in different Ti−O−Ti chains. Thus, from the perspective of a doping strategy, one may first prepare low-concentration N-doped TiO_2 sample 1, and then introduce oxygen vacancies in reducing condition 2, and most of the introduced oxygen vacancies should be adjacent to the N atoms and in the same Ti−O−Ti chains as N atoms. After that, reintroduce N atoms into sample 3, which should mainly occupy the oxygen vacancies introduced in procedure 2. By carrying out procedures 2 and 3 alternatively, there is great probability that one can finally introduce Ti−N−Ti chains into TiO_2.

The structural changes induced by substituting N for O are quite minor for all of the doping models considered here. The typical equatorial and axial Ti−N (O) bond lengths along with the corresponding bond angles before and after doping are listed in Table 1. Overall, the changes of equatorial and axial bond lengths and bond angles are within 1.5%, 4.2%, and 4.2%

Table 1. Local Bond Lengths (in Å) and Bond Angles (in deg) for the N-Doped Models[a]

models	equatorial bond	axial bond	angle 1	angle 2
pure	1.927	1.986	101.538	156.925
N-I	1.924	2.029	101.060	157.880
N-II	1.942	2.061	99.270	161.460
N-III	1.948	2.062	98.901	162.224
N-far	1.956	2.070	98.249	163.501

[a]Note that the bonds and angles correspond to those shown in Figure 1.

of the original ones, respectively. As far as we know, there are no experimental reports about the specific bond lengths of N-doped samples. However, the bond lengths in this work are in agreement with previous theoretical results.[16,17] Astonishingly, we note that the structural changes become smaller as the dopant concentration increases in our special doping arrangements. In the following we shall show that the regular structures of N-I are very important for the efficient electronic coupling between adjacent dopants, which affects the structural changes in turn. It is also noteworthy that the structural changes for N-far are the largest among all of the models, which is probably due to the weaker electronic coupling between dopants in it.

The electronic structures of the four doping models, as shown in Figure 3, reveal that N-I can effectively narrow the

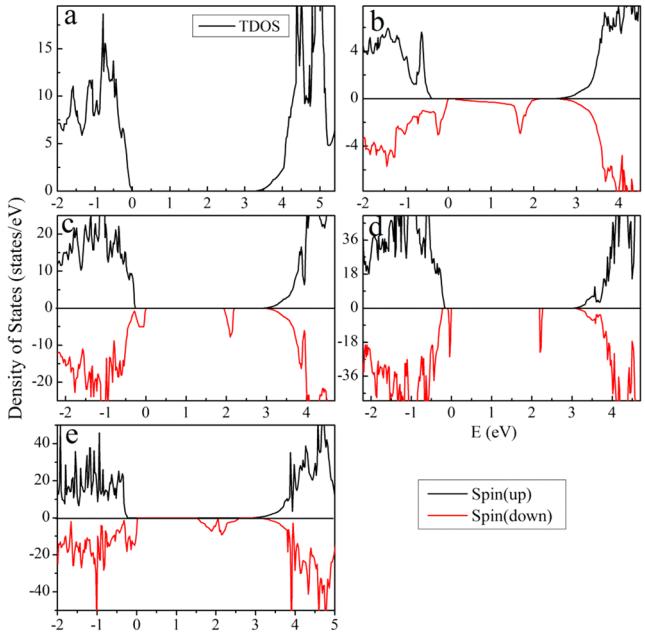

Figure 3. Density of states for (a) pure, (b) N-I, (c) N-II, (d) N-III, and (e) N-far doping models. The Fermi levels of all of the models are set to 0 eV.

band gap of TiO_2, while the other doping models mainly introduce quite localized gap states without altering the band gap. As shown in Figure 3b, the band gap of N-I is only about 2.5 eV, and the introduced gap states are very dispersive, indicating effective couplings both between neighboring N atoms and between N and host atoms. Such effective couplings can make Ti−N−Ti chains become efficient transfer channels of photogenerated carriers and also alleviate the trapping ability of gap states, thus even rendering the system infrared photocatalytic activities.[30,31] By contrast, the host electronic structures are almost unchanged in N-II, N-III, and N-far doping models, and only localized gap states positioned just above host Ev and well below Ec are induced (Figure 3c−e). These results are in line with previous theoretical reports, where only localized gap states are observed in both light and heavy N doping concentrations.[16] For the gap states positioned just above host Ev, their localized nature is reflected in the sharp decrease in the value of density of states to almost zero as they approach the host valence band edge; the localized nature of the gap states well below Ec is reflected in their narrow

distribution range. In addition, the electronic charge density distributions of the N introduced states near Ev for the four models, as shown in Figure 4, clearly show that the states are

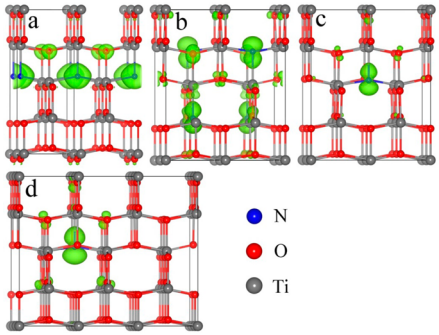

Figure 4. Electronic charge density distributions of the N introduced states near Ev for (a) N-I, (b) N-far, (c) N-II, and (d) N-III doping models. All of the isosurfaces are at 0.006 e/Å^3.

mainly composed of typical N p orbital in N-far, N-II, and N-III models, indicating again that the newly introduced gap states are isolated and mainly localized on N atoms, and this feature is also observed in previous theoretical works.[16,32] On the other hand, the electronic charge density distributions for N-I is indicative of strong sp hybridization of N orbitals, suggesting significant bonding interactions between N and adjacent Ti atoms, which will be further discussed later. Since for the four doping models the main difference among them is the mutual distance between adjacent dopants, which determines the coupling between them, the results above suggest straightforwardly the importance of electronic coupling between dopants in decreasing the band gap and enhancing the delocalization of gap states in a doped system. Finally, it is noteworthy that the calculated band gap value for the N-I model is in excellent agreement with the experimentally measured band gap of about 2.1−2.5 eV for the N-doped TiO_2 in similar doping concentration,[13,14] indicating that electronically coupled N doping may actually be favored in their doping conditions. In addition, absorption of light in the range 500−2000 nm is also observed experimentally,[14] which can be ascribed to the electron transition between the delocalized and localized states.

Because our results above indicate that the arrangement of N dopants in the shell region of the experimentally prepared core−shell structures of TiO_2 is probably the same as our N-I doping model, we further investigate its effects on photocatalytic performance and correlate our theoretical results with experimental measurements. As we know, the carrier transfer properties of a specific photocatalytic system are important for evaluating its photocatalytic performance and can be obtained from its band structures (the energy-momentum relation along high-symmetry lines in the reciprocal space). Here, we examine the band structures for pure, N-I, and N-far systems. As shown in Figure 5b, both the Ev and gap states for N-I are very dispersive, which again suggest the delocalized nature of N introduced states. Moreover, its Ev is slightly more dispersive than that of the pure system (Figure 5a), which is due to the fact that the 2p orbitals of N are more delocalized than those of O. In comparison, the band dispersion of Ev for N-far is very weak (Figure 5c), and it is much weaker than that for the pure system, thus evidently showing the localized nature of the N introduced states. For Ec of the three systems, their band dispersion is almost the same. Overall, the band dispersion above indicates that, compared to a pure system, the transfer ability of the hole is increased in N-I but decreased in N-far, and the transfer ability of electron is almost the same for the three systems. As a result, one can expect higher photocatalytic performance from the N-I doping sample.

Both the density of states and band structures for N-I above show that its band gap narrowing is mainly due to the lifting of host Ev while Ec is almost unaltered, which is consistent with the experimentally measured valence band XPS spectra.[14] To account for such behavior, the detailed electronic structures near the band edge are examined. As shown in Figure 6a, Ev is mainly composed of newly introduced N sp2 hybridized states and Ti d_{xz} states of the crystal field split t_{2g} states, where they form strong σ bonding with each other. Note that there are also appreciable amounts of O states at Ev, which are reflected in Figure 6c,d; however, for clarity they are not shown in Figure 6a. Additionally, the electronic charge density distributions of Ev also indicate that N atoms are bonding well with adjacent Ti atoms in σ-type bonds, and the adjacent N atoms show strong tendency of coupling with each other (Figure 6c,d), which is also reflected in the slight reduction of equatorial N−Ti bond lengths compared with that of corresponding O−Ti bond in pure TiO_2 (Table 1). As doping concentration decreases or the mutual distances between dopants are maximized, the tendency of dopant−dopant coupling becomes weaker or even negligible. Consequently, the overall bond lengths become larger than those in pure TiO_2, since the intrinsic bonding between Ti and N is actually weaker than that between Ti and O. Figure 6b shows that the σ antibonding states of Ti−N bonds mainly

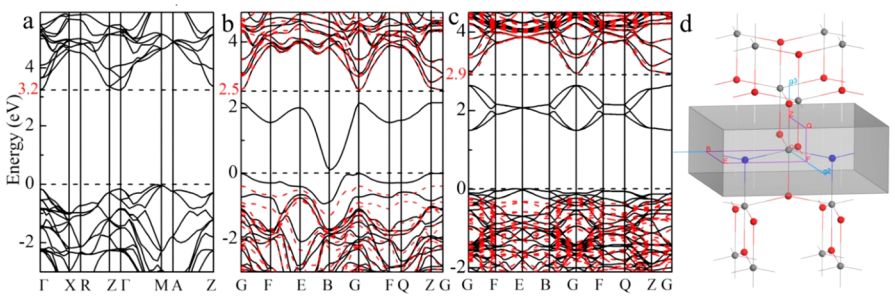

Figure 5. Energy band structures for (a) pure, (b) N-I, and (c) N-far. In parts b and c the red dashed and black solid lines are for spin-up and spin-down bands, respectively. The bands are depicted along the typical high-symmetry points of simple tetragonal crystal system for pure TiO_2; for N-I and N-far the bands are depicted along the points as shown in part d to reflect the band dispersions in planes both perpendicular and parallel to the crystal *c* axis. The Fermi levels for all of the cases are set to 0 eV, and the numerical values of conduction band edges for the three cases are shown with numbers in red.

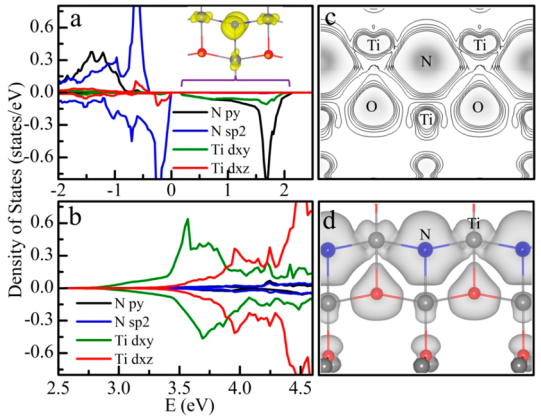

Figure 6. Orbital decomposed density of states for (a) upper valence band and gap states as well as (b) lower conduction band of N-I doping model. The atomic notations N and Ti in parts a and b refer to those indicated in part d. (c and d) The two- and three-dimensional representations of the electronic charge density distributions of upper valence band in the energy range of −0.388 to 0 eV in part a, respectively. The differences between the isolines in part c and the isosurface value in part d are 0.0005 and 0.0005 e/Å^3, respectively. The inset in part a is the electronic charge density distributions of gap states at an 0.009 e/Å^3 isosurface value. The Fermi levels in parts a and b are set to 0 eV.

composed of d_{xz} are located higher in energy than the d_{xy} states. Moreover, N p_y spin-down states slightly hybridize with the d_{xy} states of Ti atom bonding with N (Figure 6a); thus, their antibonding states mainly composed of d_{xy} states should be located higher in energy than the original nonbonding d_{xy} states, which form host Ec.[32] Taken together, all of the antibonding states involving N hardly affect the host Ec.

On the basis of the results above, we can also conclude that the overall band gap narrowing and the high dispersion of Ev are mainly due to the effective couplings both between atoms in the same Ti−N−Ti chain and between Ti−N−Ti and adjacent Ti−O−Ti chains; on the other hand, in addition to the couplings between atoms in the same Ti−N−Ti chain and between Ti−N−Ti and adjacent Ti−O−Ti chains, the couplings between adjacent Ti−N−Ti chains may also give certain contribution to the high dispersion of gap states, since the p_y hybridization between N atoms in adjacent Ti−N−Ti chains may be efficient. All of these are further confirmed by the fact that when the distance between adjacent Ti−N−Ti chains becomes twice as long as that in the N-I model, the overall band gap narrowing is actually almost unchanged, while the dispersion of gap states is slightly decreased. Thus, we can see that the introduction of the Ti−N−Ti chain is more essential for N-doped TiO_2 to show the special electronic structures than the Ti−N−Ti layer.

Narrowing the band gap of TiO_2 by lifting host Ev and retaining Ec is very beneficial to the photocatalytic and photoelectrochemical applications of TiO_2. As a matter of fact, Ev of pure TiO_2 is much more positive than the H_2O/O_2 level of water and most oxidative ions, but Ec is just slightly more negative than the H_2O/H_2 level of water and most reductive species.[1,8] Thus, lifting Ev can not only extend the light absorption range but also retain certain oxidation capacity for doped TiO_2. Additionally, lifting Ev makes the oxidation potential of TiO_2 approach that of most organic molecules and oxidative ions, which can promote the hybridization of donor and acceptor states and thereby facilitate the participation of holes in photocatalytic reactions.[33−36] On the contrary, if Ec is lowered to extend light absorption range, its reduction capacity can be seriously damaged, which may even render the sample completely inactive in the photocatalytic process.

For the electronically coupled N-I doping model, the most unexpected result is that photogenerated electrons and holes will flow in opposite directions. As shown in Figure 7b, the

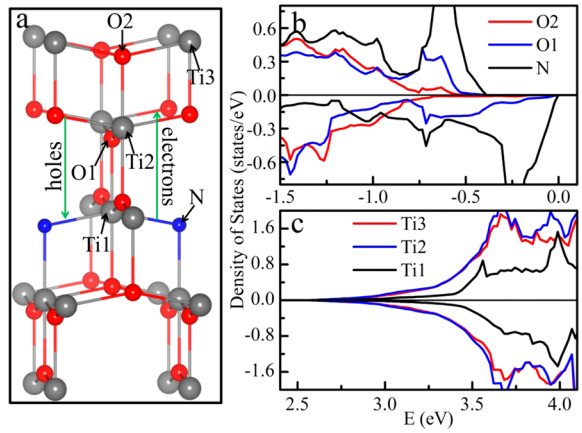

Figure 7. (a) Crystal structures of N-I doping model. (b and c) The atomic decomposed density of states for the valence and conduction band edges, respectively. The atomic notations in parts b and c correspond to those indicated in part a.

relative energies for the p states of N, O1, and O2 (Figure 7a), which are the states of photogenerated holes, are in the following order: N(p) > O1(p) > O2(p). Thus, they can provide a driving force promoting the flow of photogenerated holes from neighboring Ti−O−Ti chains to the Ti−N−Ti chains. For photogenerated electrons they have to flow oppositely, since the relative energies for the unoccupied d states of Ti1, Ti2, and Ti3 (Figure 7a) satisfy the order Ti1(d) > Ti2(d) ≈ Ti3(d) (Figure 7c). The intriguing properties of photogenerated holes and electrons can be understood as follows: Since N p states lie higher in energy than those of O, the relative energies of corresponding hole states also change accordingly; the bonding between N p_y spin-down component and Ti1 d_{xy}, as shown in Figure 6a, slightly lifts their antibonding states mainly composed of Ti d_{xy}, thus inducing flow of electrons from the Ti−N−Ti chains to the neighboring Ti−O−Ti chains. Such flow of photogenerated electrons and holes in opposite directions can separate them well spatially upon their generation, thereby decreasing recombination rate of photogenerated carriers. This can contribute to enhanced photocatalytic performance under both visible and ultraviolet light irradiation, as observed experimentally.[14]

The beneficial effects of electronically coupled N-doping on photocatalytic performance have been shown above. Here, we further investigate the factors which may affect the effective electronic couplings between dopants. In principle, assuming the same doping structures, the electronic couplings between dopants are stronger if the atomic orbital of the doped element becomes more delocalized. Therefore, larger band gap narrowing should be expected. To validate this expectation, we calculate the electronic structures of sulfur (S) (whose orbital is more delocalized than that of N) doped TiO_2 with the same doping structures as that of N-I and N-III, which are denoted as S-I and S-III, respectively. As shown in Figure 8a, the band gap of S-I is decreased to only 1.60 eV. Moreover,

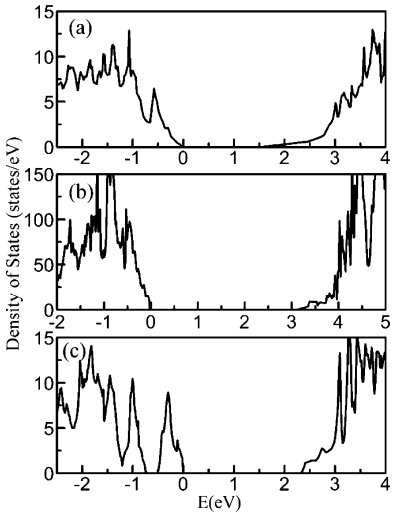

Figure 8. (a) Total density of states for S-I doping model with the same geometrical structures as that of N-I. (b) Total density of states for S-III doping model with the same geometrical structures as that of N-III. (c) Total density of states for S-I doping model with the geometrical structures fully optimized.

since the S-III doping model, which corresponds to the light doping case, hardly affects the electronic structures of pure TiO_2 and only introduces localized gap states (Figure 8b), the appreciable reduction of band gap must be mostly attributed to the stronger electronic couplings both between dopants and between dopant and host atoms, thus validating our prediction. Last but not least, as the atomic radius of S is actually much larger than O (1.09 vs 0.65 Å), large structural distortions are induced when the S-I model is optimized, which significantly destroy the effective coupling between dopants. As a consequence, only localized gap states are introduced, as shown in Figure 8c. These results obviously indicate the importance of structural regularity, in addition to the dispersiveness of the atomic orbital of the doped element, in ensuring the effective couplings both between dopants and between dopant and host atoms. Therefore, the regular structure of N-doped TiO_2 is one of the important prerequisites for the efficient couplings both between N atoms and between N and host atoms.

Generally, the electronic structures from DFT calculations depend strongly on the functionals selected. In combination with the results shown above, the different conclusions about N-doped TiO_2 in the literature should mainly originate from the different models and methods used to conduct calculations, which can lead to different electronic couplings between dopants. For example, in the previous calculations of Asahi et al.[8] the model they used probably also leads to Ti−N−Ti chains as in our N-I model; thus, notable bandgap reduction due to widening of the valence band is observed in their work. As for why no gap states appear, the conventional LDA-DFT is used in their calculations; it can overly delocalize the O and N p orbitals and thus spuriously enhance their interactions through p orbitals,[29] and unreasonably lifts the valence band edge,[37] finally making the gap states hybridize with host valence band. On the other hand, the models used in the following theoretical studies are similar to N-far, N-II, or N-III; thus, only introduction of localized gap states is reported despite many kinds of functionals, including LDA, GGA and HSE, being used.[8,16−18]

Given the experimentally prepared core−shell structures of TiO_2 nanocrystal, we further investigate the effects of such pure/N-I homostructure on photocatalytic performance. We first align the electronic structures for N-I with pure TiO_2. Also, the results show that a perfect type-II like homojunction between them is formed (Figure 9). Thus, it can promote the

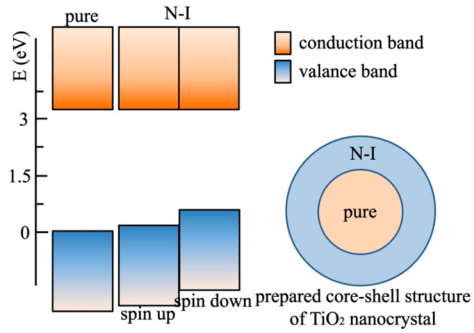

Figure 9. Aligned energy bands for the core (pure TiO_2) and shell (N-I doping model) structure of TiO_2 nanocrystal. Note that the spin-down energy band of N-I doping model is markedly lifted by 0.66 eV relative to that of pure TiO_2, while the spin-up component is only lifted by 0.27 eV.

directional flow of photogenerated holes from the core to shell region, which can further decrease the recombination of photogenerated carriers. This is also demonstrated in $CdS_{1-x}Se_x$ and $Ga_{1-x}Al_xAs$.[38−40] Furthermore, it needs to be emphasized that the effective couplings both between dopants and between dopant and host atoms in the N-I model mainly lift the spin-down component of the valence band, resulting in an energy difference between spin-down and spin-up holes (Figure 9). Such energy difference will promote the formation of more triplet electronic states for the photogenerated carriers, if the spin symmetry of the sample is broken at the interface and intersystem crossing between triplet and singlet states is allowed.[41] This can further decrease the recombination of photogenerated carriers, because the triplet states of photogenerated electron−hole pairs have a long radiative lifetime due to the spin-forbidden nature of the transition.

On the basis of the analysis above and in terms of light absorption, recombination of carriers and ease for the carriers to take part in photocatalysis, some general superiorities of such special core−shell structure of heavily N-doped TiO_2 over conventional heavily bulk-doped TiO_2 can be obtained as follows: For the heavily bulk doped TiO_2, it may extend light absorption range, but the decrease of recombination rate of photogenerated carriers is generally very limited. However, for the special core−shell structure of heavily N-doped TiO_2, in addition to having the same beneficial effects as those of a heavily bulk doped one, it can provide an additional degree of freedom to further decrease the recombination rate of photogenerated carriers, because of the band alignment between the pure core and heavily doped shell. Moreover, as noted above, the elevated valence band of the shell, where photocatalytic reactions take place, can facilitate the participation of photogenerated carriers in photocatalysis. Taken together, it is believed that the heavily doped core−shell structure of TiO_2 has the potential to show superior photocatalytic activity over heavily bulk doped TiO_2.

CONCLUSION

In summary, a systematic study of the effects of N doping on the electronic structures of TiO_2 is carried out by taking both the conventional doping wisdom and electronically coupled N doping arrangement into account and using advanced first-principles calculations. Here, the electronically coupled N doping is ensured by introducing Ti−N−Ti chains into TiO_2. First, the stability of such a special doping arrangement is verified by molecular dynamics calculations. Then, we put forward feasible strategies to prepare such electronically coupled N-doped TiO_2 experimentally. Compared to the conventional doping models, where the electronic couplings between dopants are very weak and only localized gap states are introduced, the electronically coupled N doping of TO_2 can not only significantly decrease the host band gap from 3.2 to 2.5 eV by lifting host Ev while retaining Ec, but also decrease the recombination of photogenerated carriers by both increasing the transfer ability of holes and promoting flow of photogenerated electrons and holes in opposite directions. Furthermore, the electronic couplings between dopants are shown to depend strongly on the mutual distance between dopants, the dispersion of the atomic orbital of dopant, and the structural regularity of doped system. On the basis of the results above, the distinct conclusions about N-doped TiO_2 in the literature are mainly attributed to the different models and methods used to conduct calculations, which can lead to different electronic couplings between dopants.

Overall, the results based on electronically coupled N doping model agree well with the experimental XPS and PL spectra measurements, and fully explain the reported photocatalytic properties of the core−shell structure of TiO_2.[14] In the special TiO_2 structure composed of pure TiO_2 core and the present electronically coupled N-doped TiO_2 shell, type-II like homojunction between core and shell can be formed, which can further decrease the recombination of carriers. Additionally, the general superiorities of such special core−shell structure of heavily doped TiO_2 over conventional heavily bulk-doped TiO_2 are discussed.

AUTHOR INFORMATION

Corresponding Author

*E-mail: daiy60@sina.com.

Notes

The authors declare no competing financial interest.

ACKNOWLEDGMENTS

This work is supported by the National Basic Research Program of China (973 program, 2013CB632401), National Science Foundation of China (grants 11374190 and 21333006), and 111 Project B13029. We also thank the National Supercomputer Center in Jinan for providing high performance computation.

REFERENCES

(1) Gratzel, M. Photoelectrochemical Cells. *Nature* **2001**, *414*, 338−344.

(2) Xu, M.; Gao, Y.; Moreno, E. M.; Kunst, M.; Muhler, M.; Wang, Y.; Idriss, H.; Wöll, C. Photocatalytic Activity of Bulk TiO_2 Anatase and Rutile Single Crystals Using Infrared Absorption Spectroscopy. *Phys. Rev. Lett.* **2011**, *106*, 138302.

(3) Li, X.; Li, Z.; Yang, J. Proposed Photosynthesis Method for Producing Hydrogen from Dissociated Water Molecules Using Incident Near-Infrared Light. *Phys. Rev. Lett.* **2014**, *112*, 018301.

(4) Chen, X.; Mao, S. S. Titanium Dioxide Nanomaterials: Synthesis, Properties, Modifications, and Applications. *Chem. Rev.* **2007**, *107*, 2891−2959.

(5) Dozzi, M. V.; Selli, E. Doping TiO_2 with p-Block Elements: Effects on Photocatalytic Activity. *J. Photochem. Photobiol., C* **2013**, *14*, 13−28.

(6) Ma, X.; Dai, Y.; Guo, M.; Huang, B. Relative Photooxidation and Photoreduction Activities of the {100}, {101}, and {001} Surfaces of Anatase TiO_2. *Langmuir* **2013**, *29*, 13647−13654.

(7) Di Valentin, C.; Finazzi, E.; Pacchioni, G.; Selloni, A.; Livraghi, S.; Paganini, M. C.; Giamello, E. N-Doped TiO_2: Theory and Experiment. *Chem. Phys.* **2007**, *339*, 44−56.

(8) Asahi, R.; Morikawa, T.; Ohwaki, T.; Aoki, K.; Taga, Y. Visible-Light Photocatalysis in Nitrogen-Doped Titanium Oxides. *Science* **2001**, *293*, 269−271.

(9) Yang, K.; Dai, Y.; Huang, B.; Whangbo, M.-H. Density Functional Characterization of the Band Edges, the Band Gap States, and the Preferred Doping Sites of Halogen-Doped TiO_2. *Chem. Mater.* **2008**, *20*, 6528−6534.

(10) Ma, X.; Dai, Y.; Yu, L.; Huang, B. Noble-Metal-Free Plasmonic Photocatalyst: Hydrogen Doped Semiconductors. *Sci. Rep.* **2014**, *4*, 3986.

(11) Ma, X.; Dai, Y.; Yu, L.; Huang, B. New Basic Insights into the Low Hot Electron Injection Efficiency of Gold-Nanoparticle-Photosensitized Titanium Dioxide. *ACS Appl. Mater. Interfaces* **2014**, *6*, 12388−12394.

(12) Hoang, S.; Guo, S.; Hahn, N. T.; Bard, A. J.; Mullins, C. B. Visible Light Driven Photoelectrochemical Water Oxidation on Nitrogen-Modified TiO_2 Nanowires. *Nano Lett.* **2011**, *12*, 26−32.

(13) Burda, C.; Lou, Y.; Chen, X.; Samia, A. C. S.; Stout, J.; Gole, J. L. Enhanced Nitrogen Doping in TiO_2 Nanoparticles. *Nano Lett.* **2003**, *3*, 1049−1051.

(14) Lin, T.; Yang, C.; Wang, Z.; Yin, H.; Lu, X.; Huang, F. Q.; Lin, J.; Xie, X.; Jiang, M. Effective Nonmetal Incorporation in Black Titania with Enhanced Solar Energy Utilization. *Energy Environ. Sci.* **2014**, *7*, 967−972.

(15) Asahi, R.; Morikawa, T.; Irie, H.; Ohwaki, T. Nitrogen-Doped Titanium Dioxide as Visible-Light-Sensitive Photocatalyst: Designs, Developments, and Prospects. *Chem. Rev.* **2014**, *114*, 9824−9852.

(16) Di Valentin, C.; Pacchioni, G.; Selloni, A. Origin of the Different Photoactivity of N-Doped Anatase and Rutile TiO_2. *Phys. Rev. B* **2004**, *70*, 085116.

(17) Yang, K.; Dai, Y.; Huang, B. Study of the Nitrogen Concentration Influence on N-Doped TiO_2 Anatase from First-Principles Calculations. *J. Phys. Chem. C* **2007**, *111*, 12086−12090.

(18) Varley, J. B.; Janotti, A.; Van de Walle, C. G. Mechanism of Visible-Light Photocatalysis in Nitrogen-Doped TiO_2. *Adv. Mater.* **2011**, *23*, 2343−2347.

(19) Chang, S.-m.; Liu, W.-s. The Roles of Surface-Doped Metal Ions (V, Mn, Fe, Cu, Ce, and W) in the Interfacial Behavior of TiO_2 Photocatalysts. *Appl. Catal., B* **2014**, *156−157*, 466−475.

(20) Kresse, G.; Furthmüller, J. Efficient Iterative Schemes for Ab Initio Total-Energy Calculations using a Plane-Wave Basis Set. *Phys. Rev. B* **1996**, *54*, 11169−11186.

(21) Kresse, G.; Hafner, J. Ab Initio Molecular Dynamics for Liquid Metals. *Phys. Rev. B* **1993**, *47*, 558−561.

(22) Heyd, J.; Scuseria, G. E.; Ernzerhof, M. Hybrid Functionals Based on a Screened Coulomb Potential. *J. Chem. Phys.* **2003**, *118*, 8207−8215.

(23) Heyd, J.; Scuseria, G. E.; Ernzerhof, M. Erratum: "Hybrid Functionals Based on a Screened Coulomb Potential" [J. Chem. Phys. *118*, 8207 (2003)]. *J. Chem. Phys.* **2006**, *124*, 219906.

(24) Monkhorst, H. J.; Pack, J. D. Special Points for Brillouin-Zone Integrations. *Phys. Rev. B* **1976**, *13*, 5188−5192.

(25) Blöchl, P. E.; Jepsen, O.; Andersen, O. K. Improved Tetrahedron Method for Brillouin-Zone Integrations. *Phys. Rev. B* **1994**, *49*, 16223−16233.

(26) Bylander, D. M.; Kleinman, L. Energy Fluctuations Induced by the Nosé Thermostat. *Phys. Rev. B* **1992**, *46*, 13756−13761.

(27) Nosé, S. A Unified Formulation of the Constant Temperature Molecular Dynamics Methods. *J. Chem. Phys.* **1984**, *81*, 511−519.
(28) Chai, J. W.; Yang, M.; Chen, Q.; Pan, J. S.; Zhang, Z.; Feng, Y. P.; Wang, S. J. Effects of Nitrogen Incorporation on the Electronic Structure of Rutile-TiO_2. *J. Appl. Phys.* **2011**, *109*, 023707.
(29) Freysoldt, C.; Grabowski, B.; Hickel, T.; Neugebauer, J.; Kresse, G.; Janotti, A.; Van de Walle, C. G. First-Principles Calculations for Point Defects in Solids. *Rev. Mod. Phys.* **2014**, *86*, 253−305.
(30) Tian, J.; Sang, Y.; Yu, G.; Jiang, H.; Mu, X.; Liu, H. A Bi_2WO_6-Based Hybrid Photocatalyst with Broad Spectrum Photocatalytic Properties under UV, Visible, and Near-Infrared Irradiation. *Adv. Mater.* **2013**, *25*, 5075−5080.
(31) Wang, G.; Huang, B.; Ma, X.; Wang, Z.; Qin, X.; Zhang, X.; Dai, Y.; Whangbo, M.-H. $Cu_2(OH)PO_4$, a Near-Infrared-Activated Photocatalyst. *Angew. Chem., Int. Ed.* **2013**, *52*, 4810−4813.
(32) Asahi, R.; Taga, Y.; Mannstadt, W.; Freeman, A. J. Electronic and Optical Properties of Anatase TiO_2. *Phys. Rev. B* **2000**, *61*, 7459−7465.
(33) Ma, X.; Dai, Y.; Guo, M.; Huang, B. Insights into the Role of Surface Distortion in Promoting the Separation and Transfer of Photogenerated Carriers in Anatase TiO_2. *J. Phys. Chem. C* **2013**, *117*, 24496−24502.
(34) Tafen, D. N.; Long, R.; Prezhdo, O. V. Dimensionality of Nanoscale TiO_2 Determines the Mechanism of Photoinduced Electron Injection from a CdSe Nanoparticle. *Nano Lett.* **2014**, *14*, 1790−1796.
(35) Yu, P.; Wen, X.; Lee, Y.-C.; Lee, W.-C.; Kang, C.-C.; Tang, J. Photoinduced Ultrafast Charge Separation in Plexcitonic CdSe/Au and CdSe/Pt Nanorods. *J. Phys. Chem. Lett.* **2013**, *4*, 3596−3601.
(36) Li, Y.-F.; Liu, Z.-P.; Liu, L.; Gao, W. Mechanism and Activity of Photocatalytic Oxygen Evolution on Titania Anatase in Aqueous Surroundings. *J. Am. Chem. Soc.* **2010**, *132*, 13008−13015.
(37) Janotti, A.; Varley, J. B.; Rinke, P.; Umezawa, N.; Kresse, G.; Van de Walle, C. G. Hybrid Functional Studies of the Oxygen Vacancy in TiO_2. *Phys. Rev. B* **2010**, *81*, 085212.
(38) Abdi, F. F.; Han, L.; Smets, A. H. M.; Zeman, M.; Dam, B.; van de Krol, R. Efficient Solar Water Splitting by Enhanced Charge Separation in a Bismuth Vanadate-Silicon Tandem Photoelectrode. *Nat. Commun.* **2013**, *4*, 2195.
(39) Bardi, J.; Binggeli, N.; Baldereschi, A. Structural and Compositional Dependences of the Schottky Barrier in $Al/Ga_{1-x}Al_xAs$ (100) and (110) Junctions. *Phys. Rev. B* **1999**, *59*, 8054−8064.
(40) Bardi, J.; Binggeli, N.; Baldereschi, A. Pressure and Alloy-Composition Dependence of $Al/Ga_{1-x}Al_xAs$ (100) Schottky Barriers. *Phys. Rev. B* **1996**, *54*, R11102−R11105.
(41) Liao, P.; Carter, E. A. New Concepts and Modeling Strategies To Design and Evaluate Photo-Electro-Catalysts Based on Transition Metal Oxides. *Chem. Soc. Rev.* **2013**, *42*, 2401−2422.